Supplement of Atmos. Meas. Tech., 14, 1545–1559, 2021
https://doi.org/10.5194/amt-14-1545-2021-supplement

Atmospheric Measurement Techniques
Open Access
EGU

Supplement of

Airborne extractive electrospray mass spectrometry measurements of the chemical composition of organic aerosol

Demetrios Pagonis et al.

Correspondence to: Jose L. Jimenez (jose.jimenez@colorado.edu)

Chemical Purities and Suppliers

The following chemicals were used in this study: acetonitrile (Thermo Scientific, UHPLC-MS grade); ammonium nitrate (Fisher Scientific, Certified ACS); ammonium sulfate (Fisher Scientific, Certified ACS); formic acid (Ricca, >99%); levoglucosan (CHEM-IMPEX International, >99%); methanol (Sigma-Aldrich, HPLC > 99.9%); 4-nitrocatechol (Sigma-Aldrich, 97%); pinonic acid (Sigma-Aldrich, 98%); sodium iodide (Acros Organics, 99.999% trace metals basis); and water (Thermo Scientific, UHPLC-MS grade).

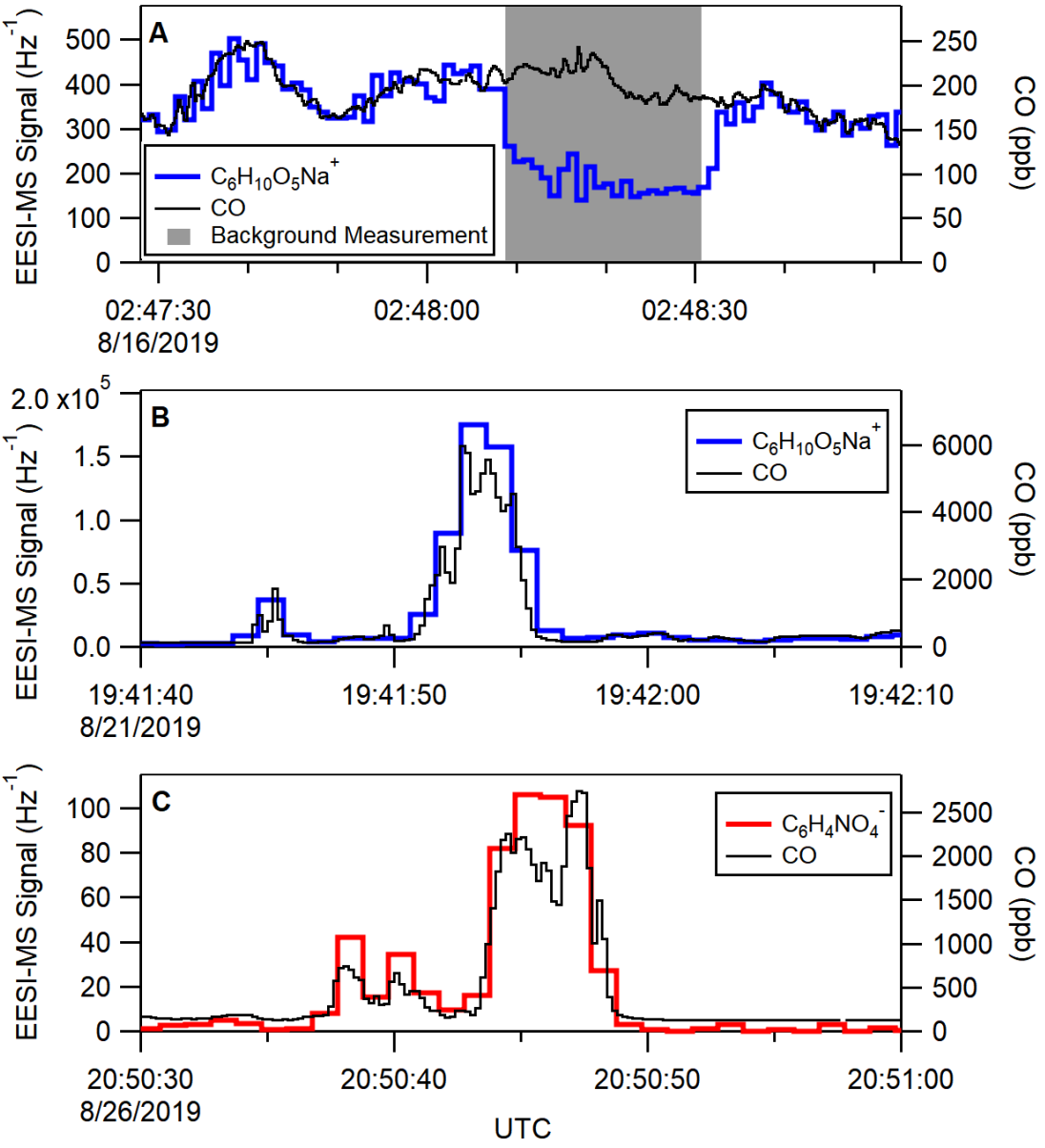

Figure S1. Response time of EESI-MS to background measurements with zero air (A), and response time during fast plume crossings in EESI(+) (B) and EESI(-) (C) operating modes. CO data is shown at 5 Hz to show plume boundaries and structure. EESI-MS response is sufficiently fast for reporting data at 1 Hz.

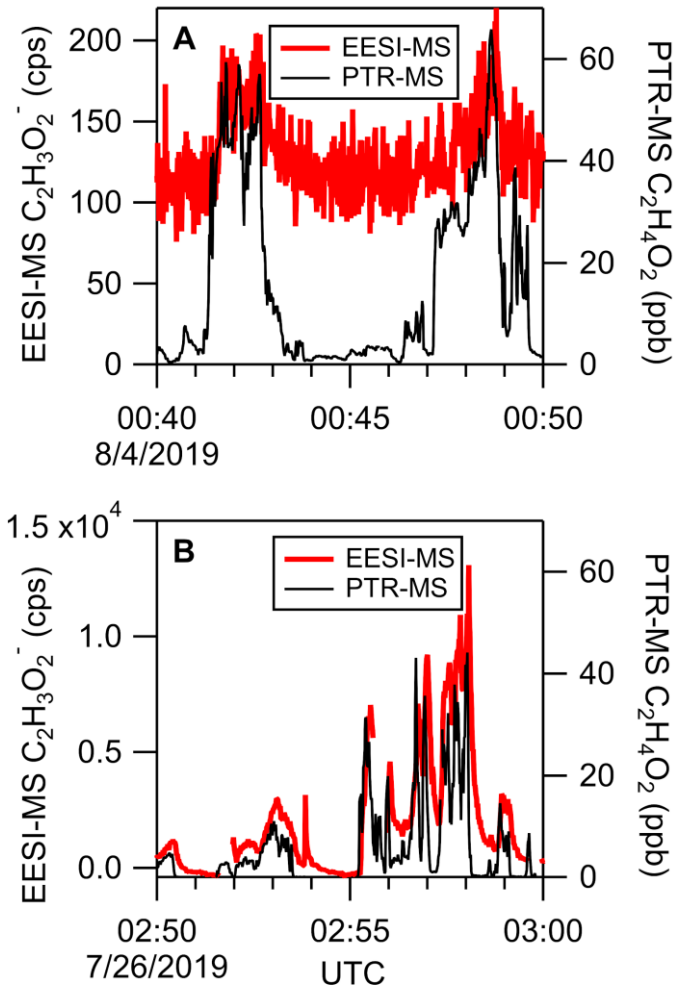

Figure S2. Quantification of EESI-MS denuder efficiency for removing gas-phase VOCs. EESI(-) acetate signal during wildfire smoke sampling with the carbon denuder in the inlet (A) and with no denuder in place (B). Comparison to PTR-MS measurements of acetic acid are included to show that similar concentrations of VOC were sampled in both example time series. Identical to Fig. 2, but with y-scaling in (A) adjusted to show the weak correlation of EESI(-) acetate with PTR-MS acetic acid.

Denuder Sorptive Capacity

Denuder sorptive capacity was estimated from the estimated geometric surface area of the denuder (207 cm^2), an assumed roughness factor of 200, and an assumed surface site density of 10^{14} sites cm^{-2}. Roughness factor was estimated from experiments measuring total VOC desorbed during bakeout of a similar denuder using PTR-MS (Bakker-Arkema and Ziemann, Personal Communication). This gives a sorptive capacity of 6×10^{18} molecules for the entire denuder, corresponding to a capacity of 3 ppm hr at 1 atm, 298 K, and 1 L min^{-1}.

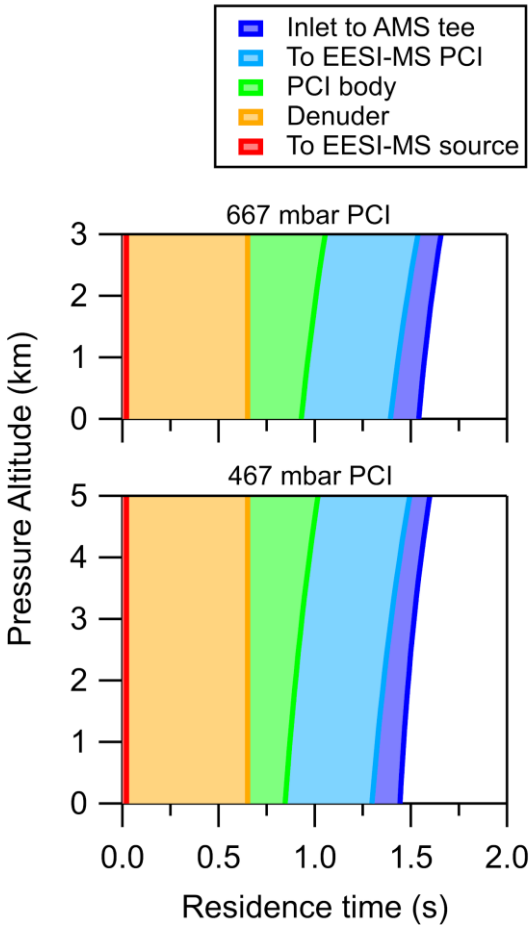

Figure S3. EESI-MS inlet residence times at PCI pressures of 467 mbar and 667 mbar as a function of sampling altitude, colored to show the contribution of each inlet subassembly.

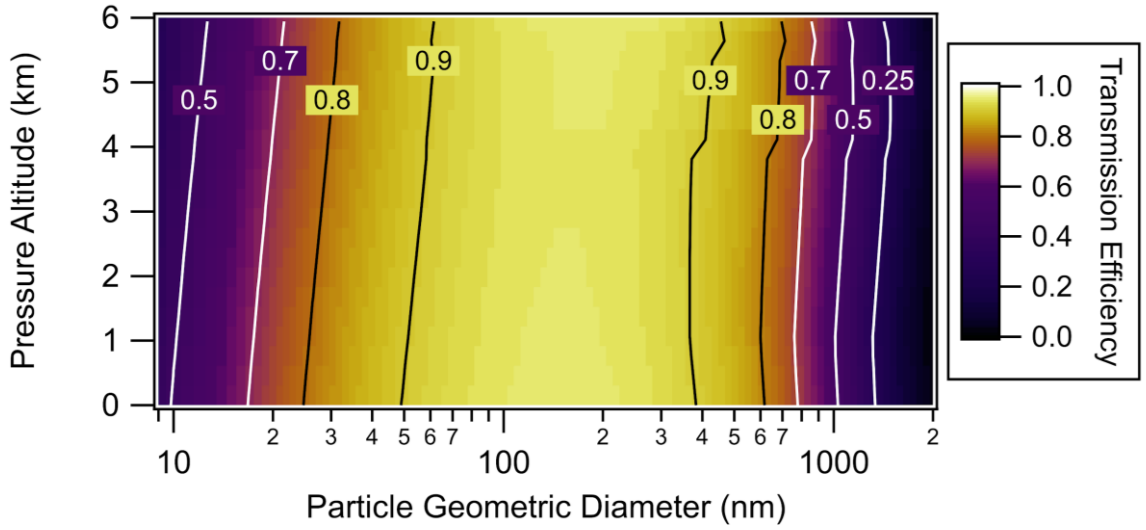

Figure S4. Calculation of particle transmission through the EESI-MS inlet as a function of sampling altitude and particle geometric diameter.

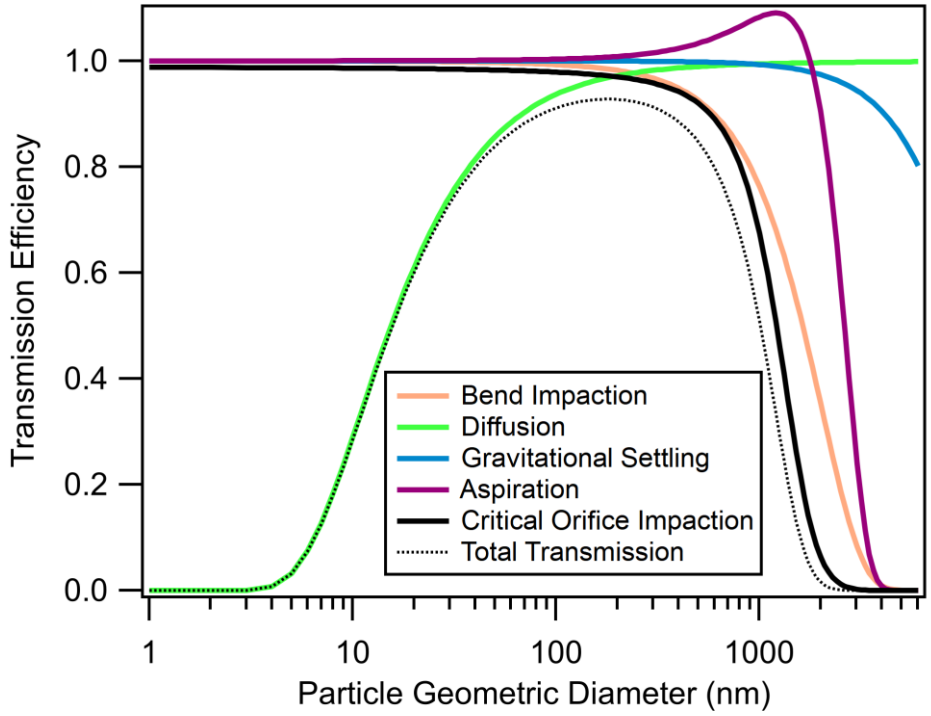

Figure S5. Estimated EESI-MS inlet transmission efficiency at a flight altitude of 1 km with respect to particle impaction in tubing bends, diffusion, gravitational settling, aspiration, and impaction behind the PCI critical orifice.

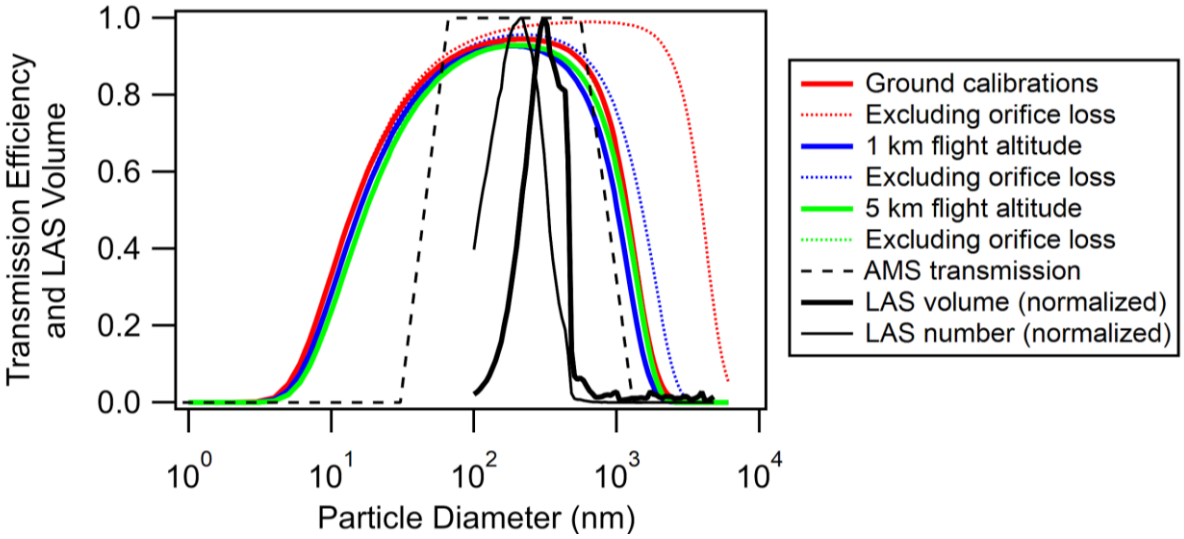

Figure S6. Estimated EESI-MS inlet transmission as a function of particle geometric diameter at representative flight altitudes and during ground calibrations. Dashed lines for EESI-MS cases show transmission for all inlet components besides the PCI critical orifice. AMS aircraft instrument transmission (Guo et al., 2020) and campaign-averaged FIREX-AQ aerosol volume and number distributions measured by laser aerosol spectrometer (LAS) are overlaid.

Critical orifice loss calculations

Particle losses from sampling through the PCI critical orifice are parameterized using the data of Chen et al. (2007). Large particle losses are dominated by deposition to the tube after the orifice. We parameterize the transmission efficiency (*TE*) in Chen et al. (2007) by Stokes number (*Stk*) using the sigmoidal function shown in Eqn. S1:

$$TE = 1 - \left(1 + e^{\frac{0.715 \times Stk^{0.5}}{0.16}}\right)^{-1} \quad \text{(S1)}$$

The critical orifice losses are roughly coincident with bend losses in the inlet, giving a 50% cutoff geometric diameter of ≈1 μm at all altitudes. During ground calibrations, the inlet is operated at a lower flow rate, reducing particle impaction losses in tubing bends. The critical orifice is then the dominant loss process for particles larger than 300 nm during ground operation, as shown in Fig. S6.

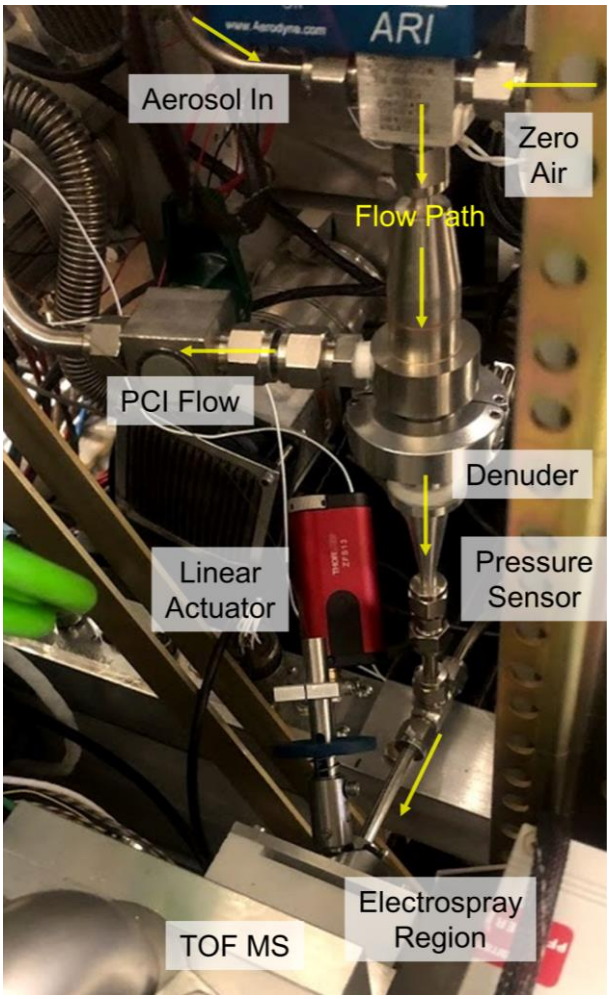

Figure S7. Photograph of the EESI-MS pressure-controlled inlet, including the linear actuator controlling the electrospray capillary position.

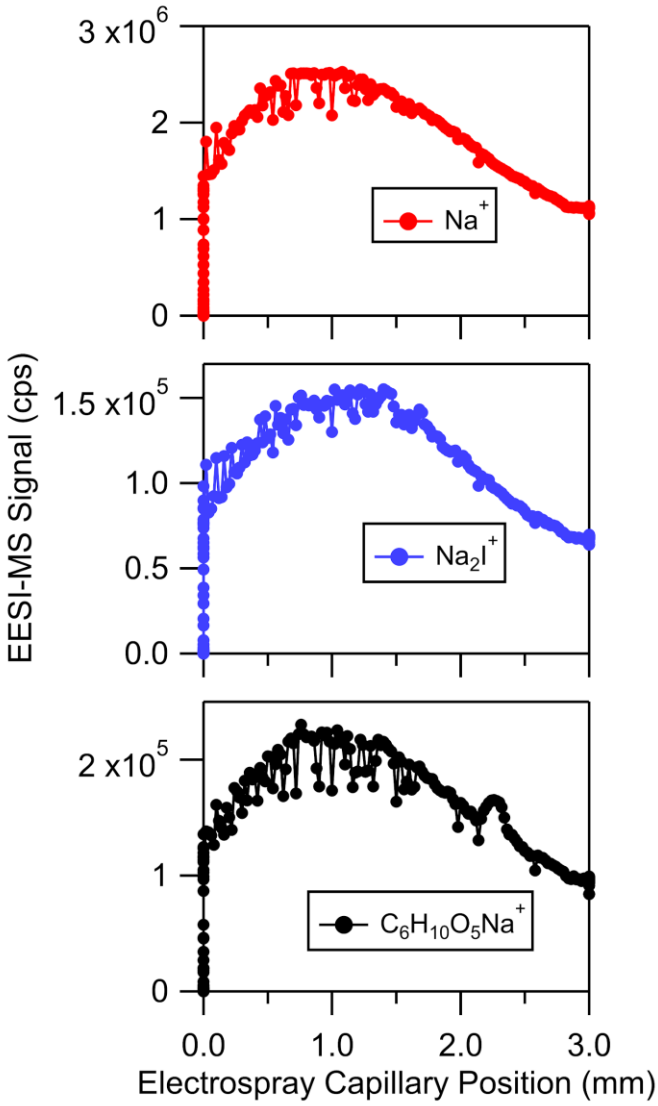

Figure S8. EESI(+) signal for primary electrospray ions and levoglucosan aerosol standard as a function of electrospray capillary position. Position 0 mm corresponds to the smallest distance between the electrospray capillary and sampling capillary where EESI-MS signal is still obtained. The position scan presented started at 3 mm and moved the electrospray capillary towards the sampling capillary (pushing electrospray capillary further into the spray region; downward in Fig. S7).

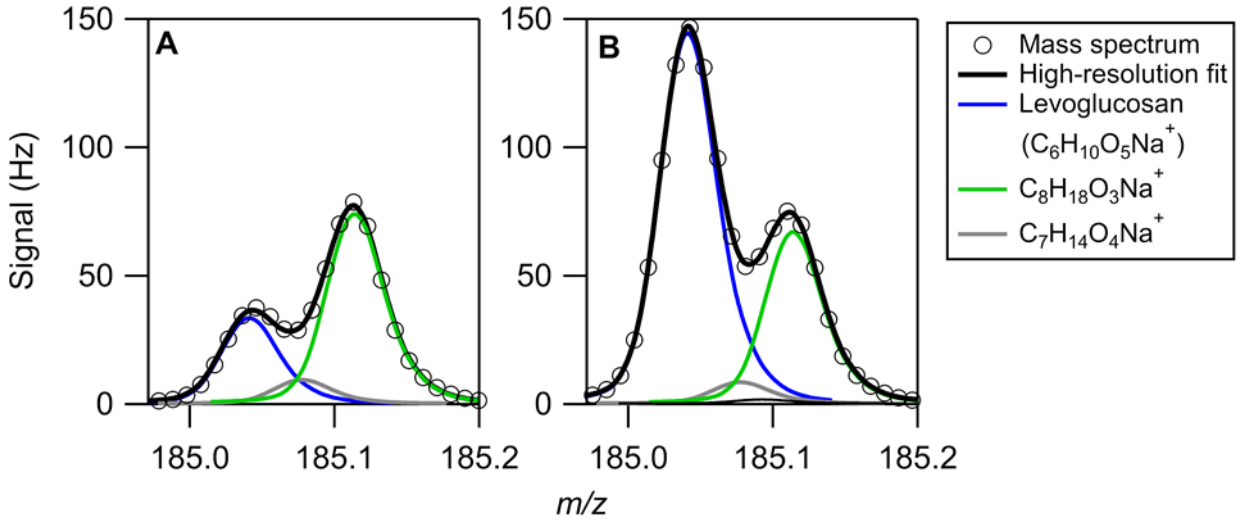

Figure S9. Levoglucosan signal during (A) measurement of instrument background and (B) sampling 50 μg sm^{-3} of smoke aerosol during a single FIREX-AQ research flight. The peak $C_6H_{10}O_5Na^+$ is resolved from the adjacent peaks.

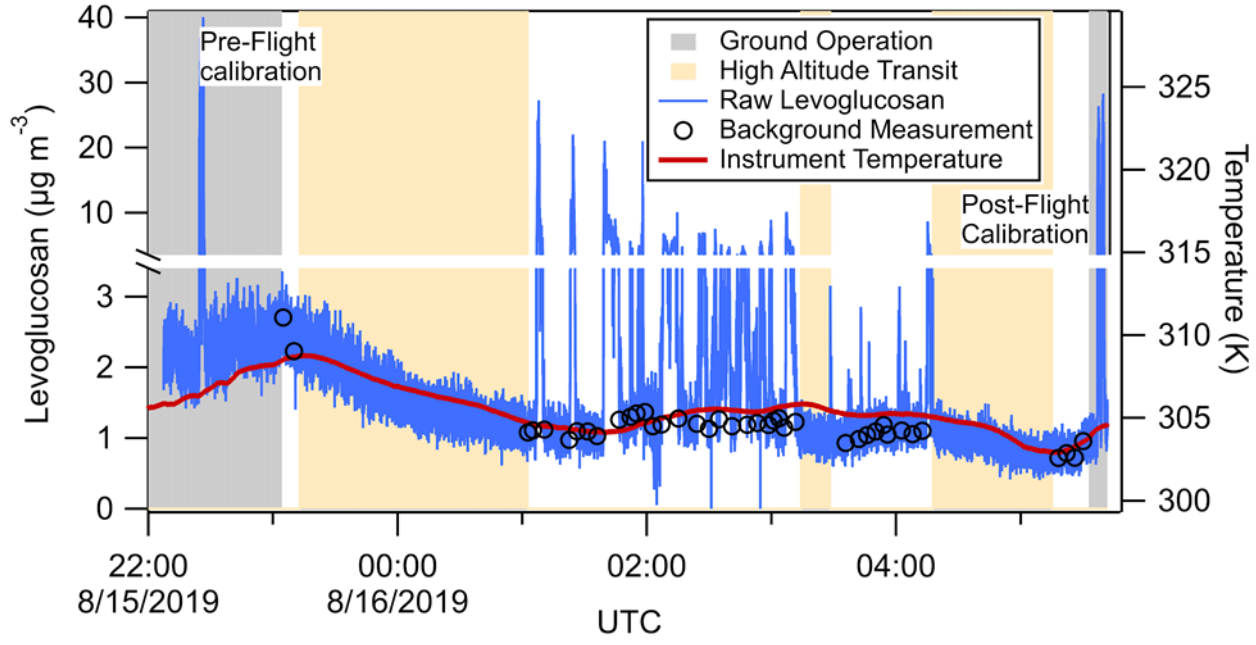

Figure S10. Raw $C_6H_{10}O_5Na^+$ signal calibrated as levoglucosan for a representative EESI(+) FIREX-AQ flight, along with average values for all background measurements. The increase in background is small following pre-flight calibration and the background prior to calibration is high, indicating that pre-flight calibrations are a minor contributor to background. The decrease in background concentration during high-altitude transits suggests that there may be accumulated levoglucosan in the EESI-MS inlet from the previous flight that slowly evaporates. This is supported by the relationship between the intensity of the background signal and instrument temperature. The small contribution of pre-flight calibrations to instrument background could be lessened through use of an isotopically labelled calibration standard. The mean and standard deviation of the background measurements are 1.2 ± 0.3 μg m^{-3}.

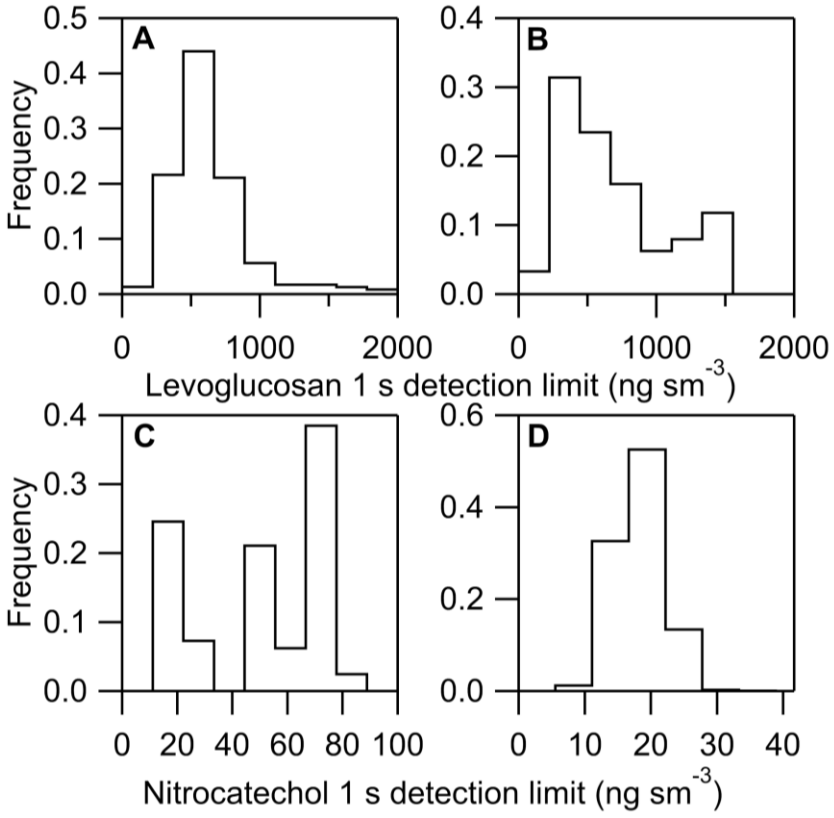

Figure S11. Histograms for EESI(+) levoglucosan and EESI(−) nitrocatechol detection limits at 1 second time resolution at (A, C) 467 mbar and (B, D) 667 mbar PCI pressure for all EESI-MS ambient sampling during FIREX-AQ. The different modes visible in (B) and (C) demonstrate the difference in performance achieved with different electrosprays. The detection limit of each electrospray varies slightly with sampling history, but the spray-to-spray variability can be larger, again demonstrating the importance of calibrating each electrospray used.

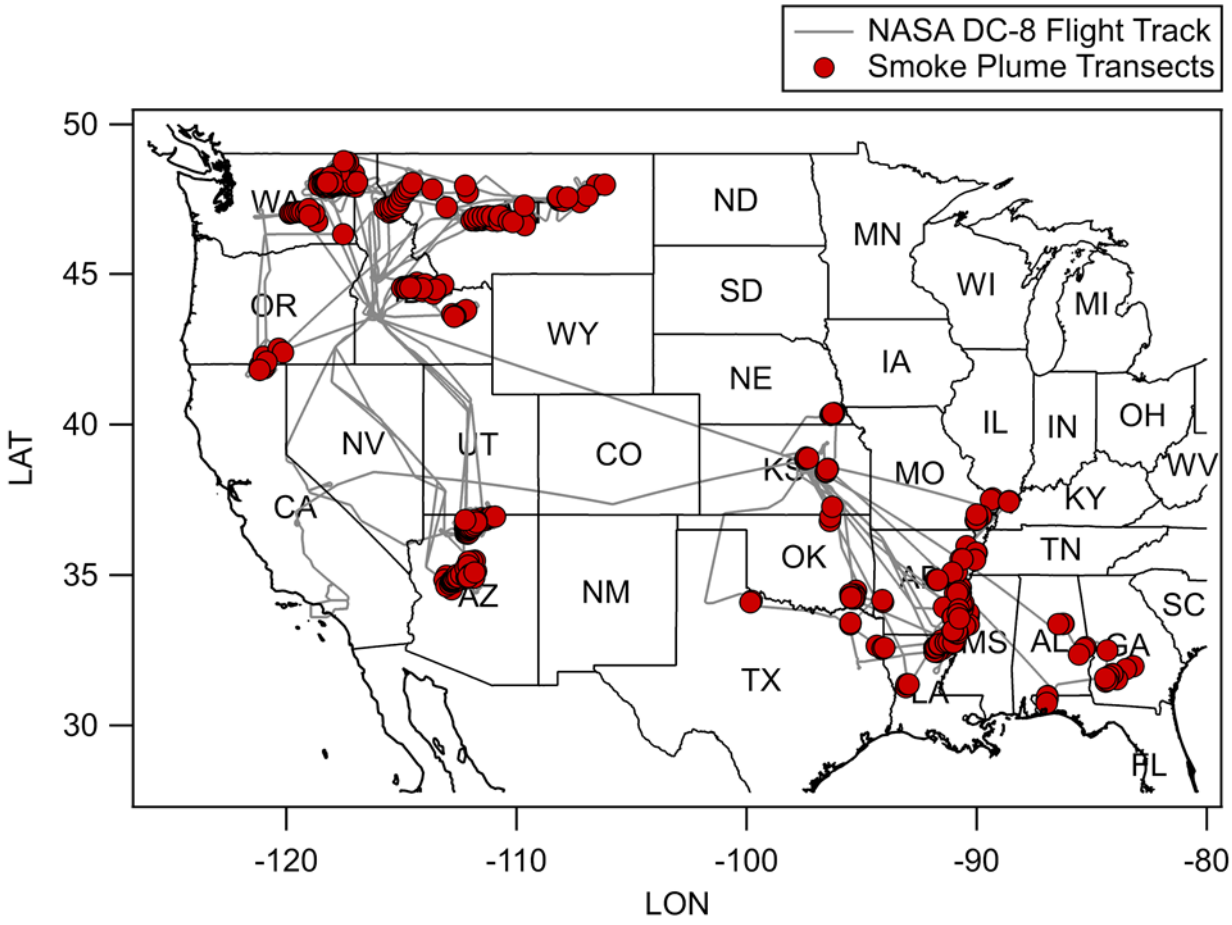

Figure S12. Flight map for the NASA DC-8 during FIREX-AQ, with smoke plume transects shown as markers.

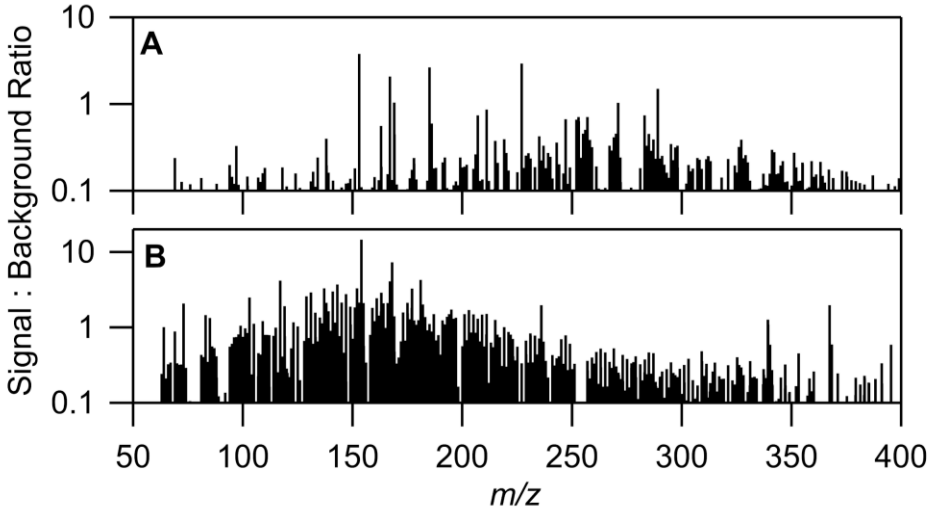

Figure S13. Signal-to-background ratio for the (A) EESI(+) and (B) EESI(-) mass spectra shown in Fig. 4. Both spectra are of 50 μg sm^{-3} of biomass burning OA.

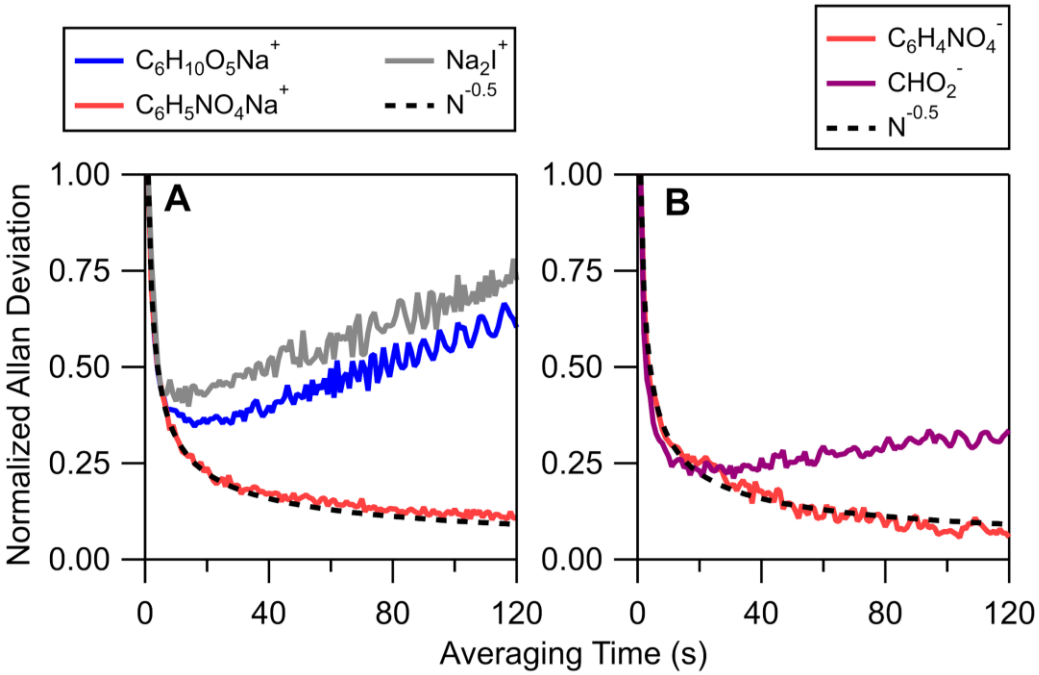

Figure S14. Allan standard deviation for (A) EESI(+) and (B) EESI(−) primary spray ions and analyte signals, calculated from extended in-flight measurements of instrument background. Signals with significant contribution from the electrospray background (e.g. primary spray ions and levoglucosan) show minima in Allan deviation near 20 s of averaging, while low-background analyte signals follow ideal counting statistics ($N^{-½}$).

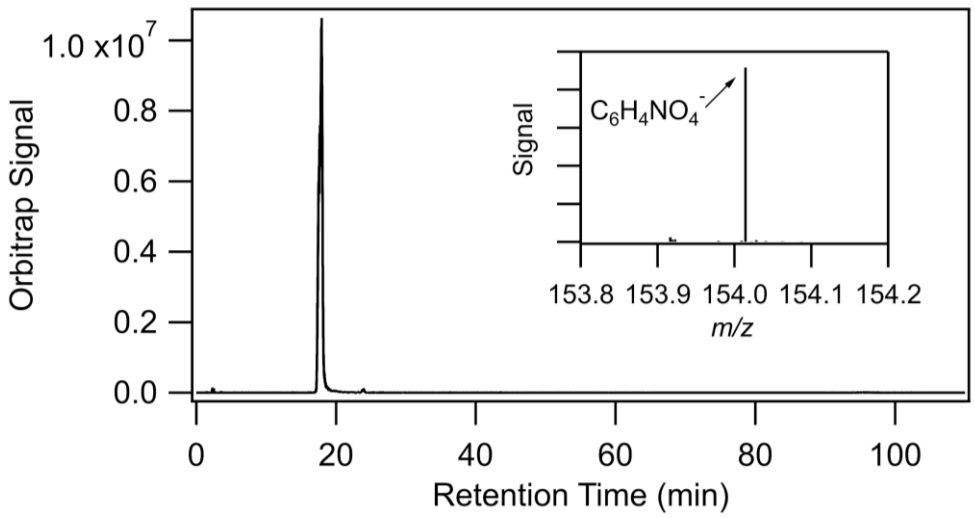

Figure S15. HPLC-ESI(−) QE Orbitrap-MS ultrahigh-resolution $C_6H_4NO_4^-$ chromatogram of a FIREX-AQ filter extract showing a single peak matching the retention time of a 4-nitrocatechol standard. Inset: average mass spectrum of the full chromatogram, showing no ESI-MS interference peaks at *m/z* 154.

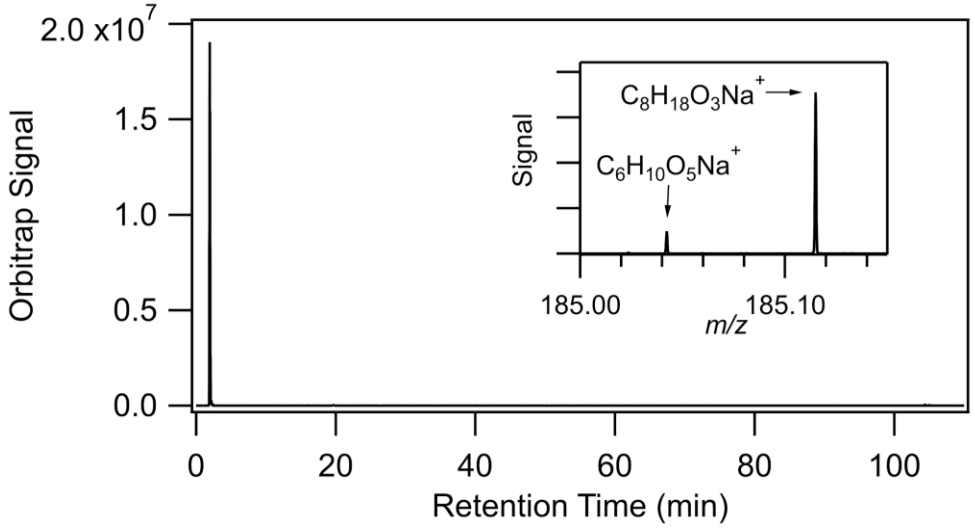

Figure S16. HPLC- ESI(+) QE Orbitrap-MS ultrahigh-resolution $C_6H_{10}O_5^+$ chromatogram of a FIREX-AQ filter extract showing a single peak matching the weakly-retained retention time of a levoglucosan standard. Inset: average mass spectrum of the full chromatogram. The background peak $C_8H_{18}O_3Na^+$ is present in both ESI-MS and EESI-MS, and is resolved from $C_6H_{10}O_5^+$ by EESI-MS, as shown in Fig. 4 and Fig. S9.

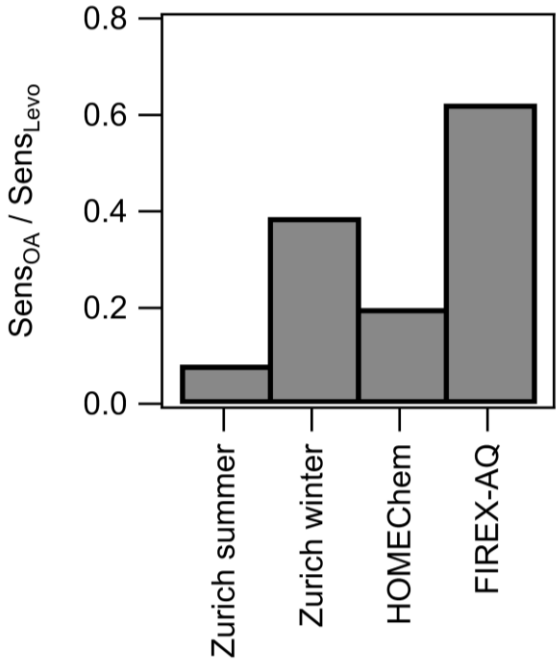

Figure S17. Comparison of EESI(+) sensitivity in this study to past EESI-MS field measurements at HOMEChem (Brown et al. 2020), as well as Zurich in summer and winter (Stefenelli et al. 2019; Qi et al. 2019). Sensitivities shown are normalized to levoglucosan sensitivity, which was used for calibration across all four studies, to account for variable electrospray region pressures and other instrument parameters. The Zurich summer and HOMEChem studies utilized a 1:1 acetonitrile:water electrospray working solutions, while the Zurich winter study utilized 1:1 methanol:water and this study utilized 3:1 methanol:water. The varying amounts of levoglucosan present track with the relative sensitivities, so it is not possible to separate the contribution of the working solution to the bulk OA sensitivity from the data available.

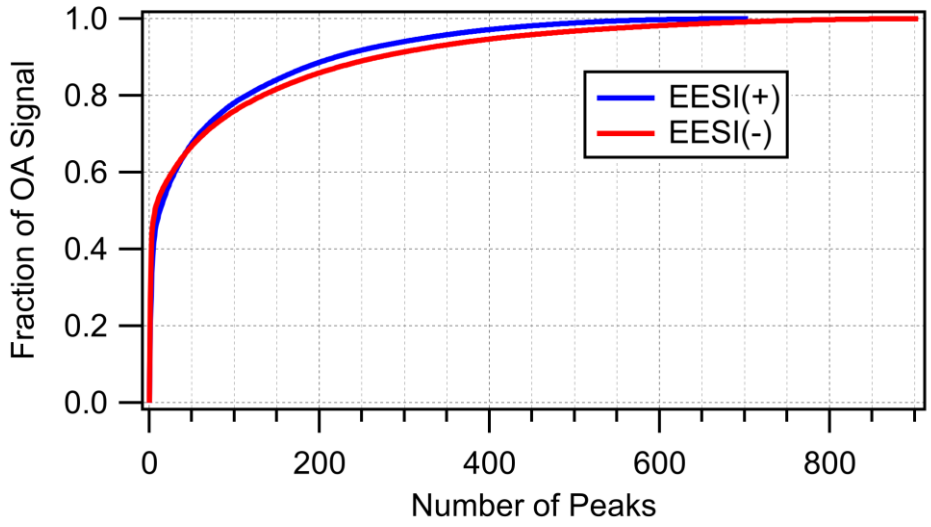

Figure S18. Cumulative fraction of OA signal as a function of the number of EESI-MS peaks giving positive signal during the research flights shown in Fig. 6. Roughly ten peaks give half the signal in both MS modes. Since EESI-MS sensitivity can vary by orders of magnitude between compounds (Lopez-Hilfiker et al. 2019; Brown et al. 2020), it is not clear whether these peaks comprise the majority of OA mass.

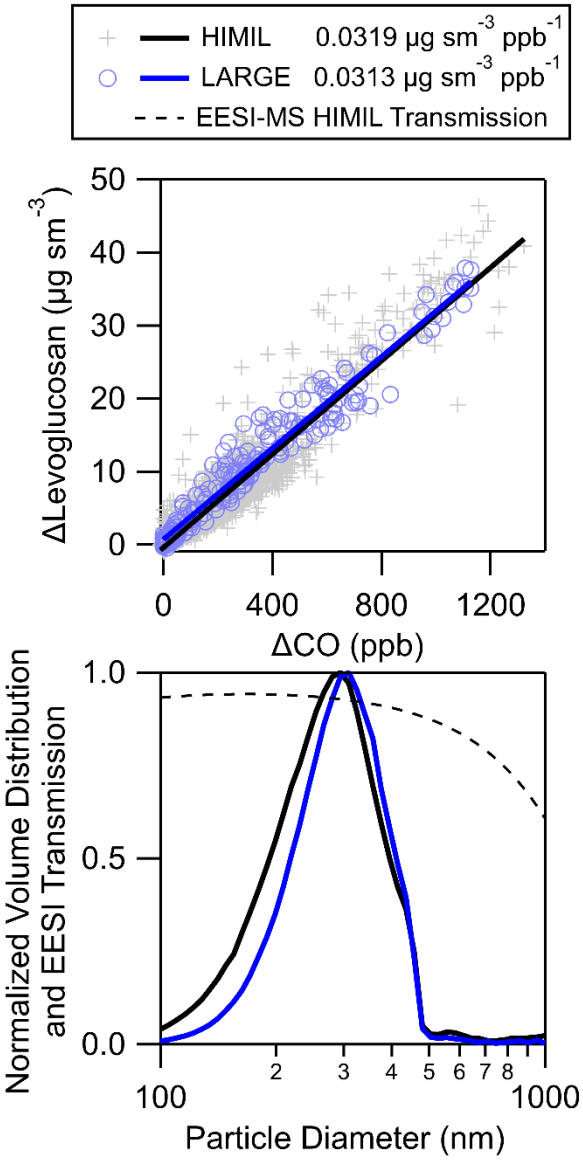

Figure S19. (A) Comparison of EESI-MS levoglucosan:CO 1 Hz emission ratios for the Sheridan fire when sampling through the HIMIL inlet and through the UH/LARGE inlet during the August 15th, 2019 research flight, and (B) the laser aerosol spectrometer size (LAS) distributions measured through the UH/LARGE inlet during the two sampling periods described in A. Identical emission ratios are measured through the two inlets. The calculated EESI-MS particle transmission at a pressure altitude of 4.7 km is shown to demonstrate that the volume distributions measured by LAS during the two sampling periods do not show any appreciable particle volume beyond the EESI-MS cutoff diameter.

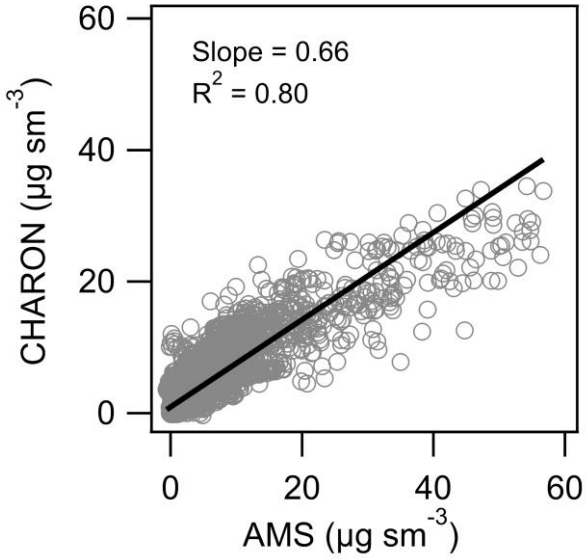

Figure S20. Comparison of 1-second CHARON PTR-MS quantification of levoglucosan to AMS levoglucosan during a single FIREX-AQ flight.

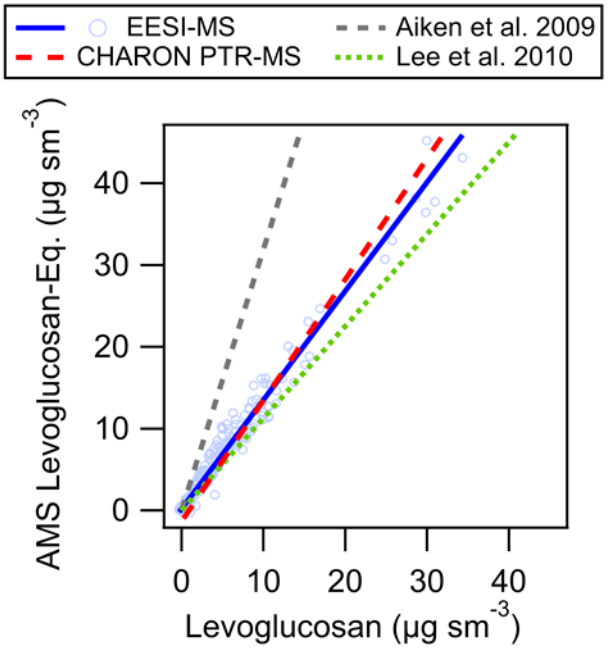

120

Figure S21. Comparison of AMS levoglucosan-equivalent to levoglucosan measured by EESI-MS (this work), CHARON PTR-MS (this work), high-performance anion-exchange chromatography of filter samples (Lee et al. 2010), and GC-MS (Aiken et al. 2009).

References

Aiken, A. C., Salcedo, D., Cubison, M. J., Huffman, J. A., De Carlo, P. F., Ulbrich, I. M., Docherty, K. S., Sueper, D., Kimmel, J. R., Worsnop, D. R., Trimborn, A., Northway, M., Stone, E. A., Schauer, J. J., Volkamer, R. M., Fortner, E., de Foy, B., Wang, J., Laskin, A., Shutthanandan, V., Zheng, J., Zhang, R., Gaffney, J., Marley, N. A., Paredes-Miranda, G., Arnott, W. P., Molina, L. T., Sosa, G. and Jimenez, J. L.: Mexico City aerosol analysis during MILAGRO using high resolution aerosol mass spectrometry at the urban supersite (T0) – Part 1: Fine particle composition and organic source apportionment, Atmos. Chem. Phys., 9, 6633–6653, 2009.

Brown, W. L., Day, D. A., Stark, H., Pagonis, D., Krechmer, J. E., Liu, X., Price, D. J., Katz, E. F., DeCarlo, P. F., Masoud, C. G., Wang, D. S., Hildebrandt Ruiz, L., Arata, C., Lunderberg, D. M., Goldstein, A. H., Farmer, D. K., Vance, M. E. and Jimenez, J. L.: Real-time organic aerosol chemical speciation in the indoor environment using extractive electrospray ionization mass spectrometry, Indoor Air, doi:10.1111/ina.12721, 2020.

Chen, S., Tsai, C., Wu, C., Pui, D. Y. H., Onischuk, A. A. and Karasev, V. V: Particle loss in a critical orifice, J. Aerosol Sci., 38(9), 935–949, 2007.

Finewax, Z., De Gouw, J. A. and Ziemann, P. J.: Identification and Quantification of 4-Nitrocatechol Formed from OH and NO3 Radical-Initiated Reactions of Catechol in Air in the Presence of NOx: Implications for Secondary Organic Aerosol Formation from Biomass Burning, Environ. Sci. Technol., 52(4), 1981–1989, 2018.

Guo, H., Campuzano-Jost, P., Nault, B., Day, D., Schroder, J., Dibb, J., Dollner, M., Weinzierl, B. and Jimenez, J.: The Importance of Size Ranges in Aerosol Instrument Intercomparisons: A Case Study for the ATom Mission, Atmos. Meas. Tech. Discuss., doi:10.5194/amt-2020-224, 2020.

Lee, T., Sullivan, A. P., MacK, L., Jimenez, J. L., Kreidenweis, S. M., Onasch, T. B., Worsnop, D. R., Malm, W., Wold, C. E., Hao, W. M. and Collett, J. L.: Chemical smoke marker emissions during flaming and smoldering phases of laboratory open burning of wildland fuels, Aerosol Sci. Technol., 44(9), doi:10.1080/02786826.2010.499884, 2010.

Lopez-Hilfiker, Felipe D., Veronika Pospisilova, Wei Huang, Markus Kalberer, Claudia Mohr, Giulia Stefenelli, Joel A. Thornton, Urs Baltensperger, Andre S. H. Prevot, and Jay G. Slowik. An Extractive Electrospray Ionization Time-of-Flight Mass Spectrometer (EESI-TOF) for Online Measurement of Atmospheric Aerosol Particles. Atmos. Meas. Tech. 12(9), 4867–86, 2019.

May, A. A., Saleh, R., Hennigan, C. J., Donahue, N. M. and Robinson, A. L.: Volatility of organic molecular markers used for source apportionment analysis: Measurements and implications for atmospheric lifetime, Environ. Sci. Technol., 46(22), 12435–12444, 2012.

Qi, L., Chen, M., Stefenelli, G., Pospisilova, V., Tong, Y., Bertrand, A., Hueglin, C., Ge, X., Baltensperger, U., Prévôt, A. S. H. and Slowik, J. G.: Organic aerosol source apportionment in Zurich using an extractive electrospray ionization time-of-flight mass spectrometer (EESI-TOF-MS) – Part 2: Biomass burning influences in winter, Atmos. Chem. Phys., 19(12), 8037–8062, 2019.

Stefenelli, G., Pospisilova, V., Lopez-Hilfiker, F. D., Daellenbach, K. R., Hüglin, C., Tong, Y., Baltensperger, U., Prévôt, A. S. H. and Slowik, J. G.: Organic aerosol source apportionment in Zurich using an extractive electrospray ionization time-of-flight mass spectrometer (EESI-TOF-MS) - Part 1: Biogenic influences and day-night chemistry in summer, Atmos. Chem. Phys., 19(23), 14825–14848, 2019.

160